Full length article

# Dust grain coagulation modelling: From discrete to continuous

P. Paruta [a,*], T. Hendrix [b], R. Keppens [b]

[a] Ecole Polytechnique Fédérale de Lausanne (EPFL), Centre de Recherches en Physique des Plasmas, Station 13, Bâtiment PPB 221, CH-1015 Lausanne, Switzerland
[b] Centre for mathematical Plasma-Astrophysics, Department of Mathematics, KU Leuven, Celestijnenlaan 200B, 3001 Heverlee, Belgium

## ARTICLE INFO

## ABSTRACT

In molecular clouds, stars are formed from a mixture of gas, plasma and dust particles. The dynamics of this formation is still actively investigated and a study of dust coagulation can help to shed light on this process. Starting from a pre-existing discrete coagulation model, this work aims to mathematically explore its properties and its suitability for numerical validation. The crucial step is in our reinterpretation from its original discrete to a well-defined continuous form, which results in the well-known Smoluchowski coagulation equation. This opens up the possibility of exploiting previous results in order to prove the existence and uniqueness of a mass conserving solution for the evolution of dust grain size distribution. Ultimately, to allow for a more flexible numerical implementation, the problem is rewritten as a non-linear hyperbolic integro-differential equation and solved using a finite volume discretisation. It is demonstrated that there is an exact numerical agreement with the initial discrete model, with improved accuracy. This is of interest for further work on dynamically coupled gas with dust simulations.

## 1. Introduction

The matter which fills the space between the stars consists of rarefied gas, small dust particles – the so called interstellar medium (ISM) – magnetic fields and background radiation. While dust accounts only for a small part of the total mass of the ISM ($\sim$1% (Spitzer, 1954)), its presence is of the utmost importance as its absorption and scattering (mainly at ultraviolet and optical wavelengths) and its (re-)emission (mainly in (far) infrared wavelengths) of incoming radiation provides the possibility to gain detailed knowledge of the ISM. Furthermore, as demonstrated in coupled gas–dust simulations of well-observed shear flow regions in the Orion nebula, performed in Hendrix et al. (2015), dust can influence the dynamics of the ISM, leading to the formation of observable structures in molecular cloud environments, in which stars and planets are ultimately formed. From recent observational data it is known that in molecular clouds, dust grains can reach micrometre scales (Pagani et al., 2010; Steinacker et al., 2010), becoming much larger than their typical size in the diffuse ISM $\sim$250 nm (Kim et al., 1994). By using adequate models of grain coagulation and accretion to simulate growth of dust grains in molecular clouds, one can try to understand the environment in

which grains grow to a substantial size, and on which time scales such growth is to be expected. In combination with observations, this allows an estimation of the life expectancy of a molecular cloud, and can even provide insight into the typical time scales of star formation processes (Hirashita and Li, 2013).

The role of dust coagulation is also important in protoplanetary disks, and in that context, it has been investigated intensely in the last decade. We limit ourselves to discuss a selection of findings that are likely also relevant for dense molecular cloud cores. Dust evolution in terms of its particle size distribution and its tendency to settle towards the midplane of a (quiescent or turbulent) protoplanetary disk was studied by Nomura and Nakagawa (2006), for the case of the solar nebula. The authors solve a coagulation equation (their Eq. (12)) that includes a vertical mass transport term of interest for dust settling in protoplanetary disks, and use it to obtain dust size distributions as a function of time and disk height at the orbits of Earth, Jupiter or Neptune. The main finding was that a gravitationally unstable layer of dust, with particles up to centimetre sizes, can form at distances 1–30 AU in a quiescent disk. Ormel et al. (2007) also investigated the solar nebula case, and used a Monte Carlo approach to, in essence, avoid the direct numerical integration of the collision/coagulation model expressed by an (extended) Smoluchowski equation (their Eq. (20)). Using Monte Carlo traces growth of individual particles directly, and can recover the evolution of the particle size distribution function, when binning over particle masses. In the

---

* Corresponding author.
  E-mail address: paola.paruta@epfl.ch (P. Paruta).

protoplanetary disk context, it was found that the collisional evolutions are influenced by the coupling between dust and gas motions, depending intricately on the internal structure of the grains (in particular, on their porosity). In the present paper, we will discuss equivalent ways to handle the direct integration of the Smoluchowski equation, inspired by the work by Hirashita (2012).

Mathematical models for grain–grain interactions have been improved in the last decade, and Hirashita's work in Hirashita and Yan (2009), Hirashita (2012) and Hirashita and Li (2013) presents discrete models for coagulation, accretion and fragmentation of dust, whilst keeping the dust decoupled from the gas dynamics. Focusing only on coagulation, the purpose of this paper is to validate the discrete model in Hirashita (2012), study its properties, and propose a different numerical implementation adapted to improve the coupling with gas dynamics. The crux of the study is the relationship identified with the well known Smoluchowski equation, introduced first in 1916 Smoluchowski (1916) and widely studied since. This result is obtained by deriving the continuous form of the discrete coagulation model in Hirashita (2012), which yields the Smoluchowski equation with a specific kernel.

The role of the Smoluchowski equation in coagulation and porosity evolution of dust species in protoplanetary disks is exploited fully in Okuzumi et al. (2009), where the distribution function of aggregates, whose evolution is governed by a Smoluchowski equation (their Eq. (1)), was allowed to depend on both mass and volume of the dust aggregates. A so-called volume-averaging procedure rephrases attention to evolution equations for the moments of the distribution function. In doing so, one needs a suitable truncation to circumvent the problem that this procedure introduces ever higher order moment dependences. In our work, we will use a simple dust coagulation model and demonstrate clearly the various equivalent means to formulate it discretely or continuously, and show the advantages of using a conservative formulation. This is needed in preparation for fully dynamic gas–dust evolutions, which simultaneously handle evolving dust size distributions. Once more, protoplanetary studies by Birnstiel et al. (2010) already made progress in handling the coupled gas plus dust evolution consistently, where a time-dependent viscous disk is incorporated as far as its radial dependences are concerned. In Birnstiel et al. (2010), the governing Smoluchowski equation was vertically integrated, using Gaussian kernels to handle some of the involved integrals analytically. A flux-conserving donor-cell scheme was then used to numerically integrate the set of two advection–diffusion equations for the surface densities of gas and dust species, together with the vertically integrated Smoluchowski equation.

The computational cost of correctly simulating dust in full 3D dynamical models (i.e. not relying on vertically integrated prescriptions) is considerable, as dust grains are highly diverse and have complex compositions and morphologies. Most importantly, they cover a size distribution range which spans more than ten orders of magnitude in locations such as protoplanetary disks (Testi et al., 2014). Only few numerical simulations have taken the effect of dust into account, and those that do have made simplifying assumptions: e.g. the works of Saito (2002), Miniati (2010) and Laibe and Price (2012) used a two-fluid approach in which only one discrete dust size is considered, while the work by Hendrix and Keppens (2014), Hendrix et al. (2015) and Hendrix and Keppens (2015) adopted a fixed size distribution for all times, where individual grain size bins do not communicate through coagulation or shattering processes, but where each size bin is coupled dynamically to the gas as a pressureless fluid subject to (size-dependent) drag-forces. This approach was pioneered in protoplanetary disk studies in Paardekooper and Mellema (2006). In an early study of protoplanetary disks, a 2.5D (axially

symmetric) model by Suttner and Yorke (2001) did explore the coupling of gas with dust using up to 30 dust size bins, and showed the importance of dust coagulation in the first 1000 years of the protostellar accretion disk.

The outline of this paper is as follows. Since we focus on a specific model as studied in discrete form by Hirashita and Li (2013), Hirashita (2012) and Hirashita and Yan (2009), we opt to summarise Hirashita's work as presented in Section 2. The corresponding continuous model is derived in Section 3. The properties of the model are then studied in Section 4, where the existence of a unique mass conserving solution is proven, relying heavily on existing literature on the Smoluchowski equation. In Sections 5 and 6, a continuously conservative alternative form is outlined, together with its finite volume approximation, following the work in Filbet and Laurençot (2004). Ultimately, the initial and the modified numerical models are compared in Section 7.

## 2. The discrete model

This section focuses on the discrete coagulation model by Hirashita (2012), which describes how dust grain size distribution $n$ evolves in time, in dense cores of molecular clouds. Discarding the spatial dynamics; which would require a coupling with the gas dynamics; it is possible to write the distribution as a function $n(a, t)$ only of particle size $a$ and time $t$. In the discrete model used in Hirashita (2012), $n$ is hidden in the discrete variable $\rho_i$ which represents the mass density of all grains with mass in the range $[m_{i-1/2}, m_{i+1/2}]$:

$$\rho_i(t) = \int_{m_{i-1/2}}^{m_{i+1/2}} \hat{n}(m, t) m \, dm \sim \hat{n}(m_i, t) m_i [m_{i+1/2} - m_{i-1/2}], \quad (1)$$

where $\hat{n}(m, t)$ is the number density as a function of the grain mass $m$ instead of the grain size, which is related to $n(a, t)$ through $dN_{gr}/V = n(a, t) \, da = \hat{n}(m, t) \, dm$, where $N_{gr}(t)$ is the total number of dust grains at time $t$ in a volume $V$. The index $i$ ranges from 1 to $N$, with $N$ the total number of dust bins in the discrete model such that $\cup_i (m_{i-1/2}, m_{i+1/2})$ covers the total interval of grain masses considered.

The discrete model for dust coagulation taken from Hirashita (2012) reads:

$$\frac{\rho_i^{n+1} - \rho_i^n}{\Delta t} = -Q^- + Q^+, \quad (2)$$

at the left hand side, an explicit Euler scheme is used for the time evolution of the discrete variable $\rho_i$ and the superscript index $n$ (here, $n$ is not the grain size distribution anymore) accounts for the time discretisation. At the right hand side, $Q^-$ represents the loss term of the $i$th bin, due to the coagulation between grains in the $i$th bin and all grain sizes. $Q^+$ instead is the gain term of the $i$th bin, given by all the interactions between smaller grains that give rise to grains of $i$th mass. These terms are all evaluated at time level $n$ (explicit) and characterised as follows

$$Q^- = m_i \rho_i \sum_{l=1}^{N} \alpha_{li} \rho_l, \quad (3)$$

$$Q^+ = \sum_{j=1}^{N} \sum_{l=1}^{N} \alpha_{lj} \rho_l \rho_j m_{coag}^{lj}(i). \quad (4)$$

In the expressions, $\alpha_{lk}$ is a weight matrix:

$$\alpha_{lk} = \frac{\sigma_{lk} v_{lk}}{m_k m_l}. \quad (5)$$

Here, $\sigma_{lk} = \pi (a_l + a_k)^2$ is the cross section, note that the sizes $a_l, a_k$ can be seen as function of grain mass $m$, since the grains are

**Table 1**

The table groups all the parameters necessary for the code, from right to left, in the first line: gas temperature, hydrogen number density, hydrogen atomic mass ($u = 1.660538921 \times 10^{-24}$ g), mass density of silicate grains, mass dust to gas ratio and the mean molecular weight. The bottom row mentions minimal grain size, maximal grain size for the initial distribution, maximal grain size considered for the simulation, and the total time simulated. For reference, the free-fall time and a year expressed in seconds are also listed. All the parameters are in accordance with (Hirashita and Li, 2013).

| $T_{gas}$ [K] | $n_H$ [cm$^{-3}$] | $m_H$ [u] | $\rho_{gr}$ [g cm$^{-3}$] | $R$ | $\mu$ |
|---|---|---|---|---|---|
| 10 | $10 \times 10^5$ | 1.00749 | 3.3 | 0.01 | 1.4 |
| $a_{min}$ [cm] | $a_{max}$ [cm] | $a_{top}$ [cm] | $T_{max}$ | $t_{ff}$ [yr] | yr [s] |
| $3 \times 10^{-7}$ | $2.5 \times 10^{-5}$ | $1.2 \times 10^{-3}$ | $10 t_{ff}$ | $1.38 \times 10^5$ | 31 556 926 |

considered spherical,[1] therefore $m = (4/3)\pi \rho_{gr} a^3$ where a typical constant grain density is $\rho_{gr}$. The quantity $v_{lk}$ stands for $v(a_l, a_k)$, which is the magnitude of the relative velocity between particles $k$ and $l$. Computing the relative velocity of two particles when space is not taken into account requires modelling. The assumption Hirashita makes is that particles do not move in a specific direction and therefore the incident collision angle $\theta$ between two particles is random:

$$v(a_i, a_j) = (v(a_i)^2 + v(a_j)^2 + 2v(a_i)v(a_j)\cos\theta)^{1/2}. \qquad (6)$$

Such formulation introduces stochasticity in the model, $\cos(\theta)$ in the above equation is in Hirashita and Li (2013) taken from a realisation of a uniform distribution in $[-1, 1]$ (which should reflect the process of randomly choosing the angle in three dimensions). From Appendix A of Ormel et al. (2009), the particle velocity is written in Hirashita and Li (2013) as a function of the size through

$$v(a) = Ca^{1/2}, \qquad (7)$$

which follows from the full dependence

$$1.1 \times 10^3 \left(\frac{T_{gas}}{10\,K}\right)^{\frac{1}{4}} \left(\frac{n_H}{10^5\,cm^{-3}}\right)^{-\frac{1}{4}}$$
$$\times \left(\frac{\rho_{gr}}{3.3\,g\,cm^{-3}}\right)^{\frac{1}{2}} \left(\frac{a}{0.1\,\mu m}\right)^{\frac{1}{2}} cm\,s^{-1}$$

under the assumption of constant gas temperature $T_{gas}$, number of hydrogen atoms $n_H$ and typical grain density $\rho_{gr}$ (listing typical values in the denominators, our Table 1 groups all parameter values we used in further computations). Note that this expression for the particle velocities as function of size and other thermodynamic parameters relates to the intermediate velocity regime, whereas in reality the relative velocities between two particles in turbulence will depend on the ordering between the particle friction times (relating to the coupling between the gas and the dust) and the (turbulent) eddy turn-over time (Ormel et al., 2009, and references therein). Here we again make specific simplifying assumptions, e.g. also assuming spherical grains that behave as compact spheres.

The last term in (4), $m_{coag}^{lj}(i)$, takes into account the fact that the gain term describes interaction between two grains of mass $m_j$ and $m_l$ such that the resulting grain is of mass $m_i$. Hence $m_{coag}^{lj}(i) = m_l$ if $m_{i-1/2} < m_j + m_l < m_{i+1/2}$, and zero otherwise. Hirashita's model in Hirashita and Li (2013) considers three possible scenarios called the *standard silicate model*, the *sticky coagulation model* and the *maximal coagulation model*, which differ by the cross section $\sigma_{lk}$ and the presence of a threshold for the relative velocity $v_{lk}$, above which no coagulation occurs. The equations reported

above correspond to the *sticky coagulation model*, chosen because it is consistent with molecular cloud physics where grains are ice-coated (*sticky*) and therefore the velocity threshold can be neglected.

## 3. From discrete to continuous

The following contains a mathematical derivation step by step of the continuous form of Eq. (2), for a better understanding of the model and its properties. The left hand side of Eq. (2) can be seen as $\frac{d\rho_i(t)}{dt}$, and using Eq. (1) it follows:

$$\frac{d}{dt}\int_{m_{i-1/2}}^{m_{i+1/2}} m\hat{n}(m, t)dm = -Q_{sc}^- + Q_{sc}^+. \qquad (8)$$

The loss term $Q_{sc}^-$ (where $sc$ stands for semi-continuous approximation), obtained by using Eq. (1) in the expression for $Q^-$, reads:

$$Q_{sc}^- = \int_{m_{i-1/2}}^{m_{i+1/2}} m\hat{n}(m, t)\,dm \int_0^\infty \sigma(m_i, \bar{m})v(m_i, \bar{m})\hat{n}(\bar{m}, t)\,d\bar{m}. \qquad (9)$$

A semi-continuous expression for $Q_{sc}^+$ is slightly more complicated to derive. From Eq. (4), $m_{coag}^{lj}(i)$ can be substituted with $m_l$ as long as the sum over $l$ is restricted to those grains whose mass $m_l$ added to $m_j$ belongs to the $i$th bin. When $I_{ij}$ denotes such set, it is possible to write:

$$Q_{sc}^+ = \sum_{j=1}^N \rho_j \sum_{l \in I_{ij}} \frac{v_{lj}\sigma_{lj}}{m_l m_j} m_l \int_{m_{l-1/2}}^{m_{l+1/2}} \tilde{m}\hat{n}(\tilde{m}, t)d\tilde{m}. \qquad (10)$$

The sum over $l$ can be re-written as an integral[2] from $m_{i-1/2} - m_j$ to $m_{i+1/2} - m_j$ (with $m_j$ smaller that $m_{i+1/2}$):

$$Q_{sc}^+ = \sum_{j=1}^i \rho_j \int_{m_{i-1/2}-m_j}^{m_{i+1/2}-m_j} \frac{v(\tilde{m}, m_j)\sigma(\tilde{m}, m_j)}{m_j} \tilde{m}\hat{n}(\tilde{m}, t)\,d\tilde{m}. \qquad (11)$$

The same can be done with $\rho_j$ and the sum over $j$:

$$Q_{sc}^+ = \int_0^{m_{i+1/2}} \bar{m}\hat{n}(\bar{m}, t)$$
$$\times \left[\int_{m_{i-1/2}-\bar{m}}^{m_{i+1/2}-\bar{m}} \frac{v(\tilde{m}, \bar{m})\sigma(\tilde{m}, \bar{m})}{\bar{m}} \tilde{m}\hat{n}(\tilde{m}, t)\,d\tilde{m}\right] d\bar{m}. \qquad (12)$$

Note that the relative velocity and the cross section are now considered as functions of the particle mass, with $\rho_{gr}$ the (constant, species-specific) mass density of the grain. The cross section $\sigma$ reads:

$$\sigma = \pi(a + \bar{a})^2 = \pi \left(\frac{3}{4\pi\rho_{gr}}\right)^{2/3} (m^{1/3} + \bar{m}^{1/3})^2, \qquad (13)$$

---

[1] The cross section expression stated here adopts a perfect sticking efficiency and is purely geometrically determined. It is conceivable to relax this assumption, as well as the one on the grains being purely spherical.

[2] Note that we do not assume that all bins have equal lengths here, but do assume that they do not overlap. We simply rewrite the discrete summations to integral form.

while the resulting expression for the velocity is explicitly:

$$v(m) = C\left(\frac{m}{\frac{4}{3}\rho_{gr}\pi}\right)^{1/6} = \tilde{C}m^{1/6}. \tag{14}$$

$\tilde{C}$ is constant and its unit measure is [cm s$^{-1}$ g$^{-1/6}$]. Note that this expression is specific for the simple turbulence model we adopted here, and more sophisticated parametrisations have been put forward, e.g. in Yan et al. (2004) where magnetic field induced anisotropy due to magnetohydrodynamic processes for charged dust grains were analysed.

In a continuous setting, the relative velocity cannot be computed through a stochastic process; it would mean doing an infinite number of realisations and it would lead to discontinuous functions which are mathematically impossible to integrate. Of course, by numerically computing the integral, the desired stochasticity could be reproduced. Nonetheless, a deterministic model is preferable and therefore the idea is to look for an upper and lower bound for analysing the relative velocity instead. The maximal relative velocity is reached when the two particles hit frontally ($\cos(\theta) = -1$):

$$v_{max}(m, \bar{m}) = \tilde{C}(m^{1/6} + \bar{m}^{1/6}). \tag{15}$$

On the other hand, the lowest relative velocity is obtained when the particles are moving (almost) parallel to each other in the same direction ($\cos(\theta) = +1$):

$$v_{min}(m, \bar{m}) = \tilde{C}|m^{1/6} - \bar{m}^{1/6}|. \tag{16}$$

The final step from semi continuous to fully continuous is carried out by dividing by $\Delta m_i = m_{i+1/2} - m_{i+1/2}$ and taking the number of bins to infinity ($\Delta m_i \to 0$).

$$\lim_{\Delta m_i \to 0} \frac{1}{\Delta m_i} \frac{d}{dt} \int_{m_{i-1/2}}^{m_{i-1/2}+\Delta m_i} m\hat{n}(m, t)\, dm$$

$$= \lim_{h \to 0} \frac{1}{\Delta m_i}(-Q_{sc}^- + Q_{sc}^+). \tag{17}$$

Since the length of the $i$th interval goes to zero in this limit process, the $i$th bin boundaries $m_{i-1/2}$ and $m_{i+1/2}$ as well as the representative bin mass $m_i$ all attain the same value, that can be simply identified with $m$. The resulting equation, after evaluating the limit, is:

$$\frac{\partial}{\partial t}\hat{n}(m, t) = -Q_c^- + Q_c^+,$$

$$Q_c^- = \hat{n}(m, t) \int_0^\infty \sigma(m, \bar{m})v(m, \bar{m})\hat{n}(\bar{m}, t)\, d\bar{m},$$

$$Q_c^+ = \int_0^m \frac{m-\bar{m}}{m}\sigma(m-\bar{m}, \bar{m})v(m-\bar{m}, \bar{m})$$

$$\times\, \hat{n}(\bar{m}, t)\hat{n}(m-\bar{m}, t)\, d\bar{m}, \tag{18}$$

where $v(m, \bar{m})$ is given by either Eq. (15) or Eq. (16). Since the mass $m$ is not time dependent, both sides have been divided by $m$.

The gain term can be further simplified exploiting the symmetry of $\sigma$ and $v$, with a change of the integration variable from $\bar{m}$ to $m - \bar{m}$:

$$Q_c^+ = \int_m^0 -\frac{\bar{m}}{m}\sigma(\bar{m}, m-\bar{m})v(\bar{m}, m-\bar{m})$$

$$\times\, \hat{n}(m-\bar{m}, t)\hat{n}(\bar{m}, t)\, d\bar{m}. \tag{19}$$

Physically this is simply a change in perspective, there are two particles merging in a particle of size $m$ and it does not matter which of the two is considered. By adding the two formulations for

$Q_c^+$ and dividing by two the mass fractions sum to unity. Eq. (18) can hence be written with the following notation:

$$\frac{\partial}{\partial t}\hat{n}(m, t) = -\hat{n}(m, t) \int_0^\infty K(m, \bar{m})\hat{n}(\bar{m}, t)\, d\bar{m}$$

$$+ \frac{1}{2}\int_0^m K(m-\bar{m}, \bar{m})\hat{n}(\bar{m}, t)\hat{n}(m-\bar{m}, t)\, d\bar{m}, \tag{20}$$

with $K(m, \bar{m}) = \sigma(m, \bar{m})v(m, \bar{m})$ and the integral over the mass of the grains limited to the range of interest. This is the well known Smoluchowski equation for coagulation, firstly introduced in 1916 in Smoluchowski (1916). All kinds of different physical processes can be reproduced only by changing the kernel $K(m, \bar{m})$ in Eq. (20). As a consequence, the kernel is what requires most of the modelling effort. The idea behind the equation, in itself, is simple: the rate of change in the grain distribution ($\partial_t \hat{n}$) of particles with mass $m$ (size can be used instead), is due to the difference between $m$ particles created by two smaller ones merging ($\{\bar{m}\} + \{m-\bar{m}\} \to \{m\}$) and $m$ particles depleted due to their coagulation into bigger grains ($\{m\} + \{\bar{m}\} \to \{m + \bar{m}\}$).

To avoid confusion, the different reformulations for the coagulation model are grouped in Table 3, where in addition to the discrete initial form and the newly derived continuous one, the conservative formulation and its numerical interpretation (presented in the upcoming Sections 5 and 6) are also gathered.

## 4. Analytical properties

In Dubovskiĭ (1994) Dubovskiĭ presents conditions for the kernel and the initial condition that allow for the existence and uniqueness of mass conserving solutions for the Smoluchowski equation enriched with a fragmentation term. The mathematical analysis in Filbet and Laurençot (2004) summarises the hypothesis and proof in case of pure coagulation. If the kernel respects the so called mild growth condition (mathematically, this condition expresses that the kernel behaves sublinearly, physically it is important to have limited growth for larger and larger mass ranges),

$$K(m, \bar{m}) \leq A(m_0 + m + \bar{m}), \quad (m, \bar{m}) \in \mathbb{R}^2, \tag{21}$$

for some $A > 0$ and reference mass $m_0$, and the initial distribution is such that:

$$\hat{n}(m, 0) \in L^1(\mathbb{R}_+; (m_0 + m)dm), \tag{22}$$

then it can be proven that Smoluchowski equations have a unique mass conserving solution. The requirement on the initial condition means that

$$\int_0^\infty \hat{n}(m, 0)(m_0 + m)dm \tag{23}$$

has to be finite. It is not hard to verify whether (21) and (22) are satisfied with Hirashita's kernel and initial conditions. The kernel is:

$$K(m, \bar{m}) = v(m, \bar{m})\sigma(m, \bar{m}) \leq v_{max}(m, \bar{m})\sigma(m, \bar{m}). \tag{24}$$

Gathering Eqs. (13) and (15) together, the following inequality for the kernel holds:

$$K(m, \bar{m}) \leq \hat{C}(m^{1/3} + \bar{m}^{1/3})^2(m^{1/6} + \bar{m}^{1/6})$$

$$\leq A(m_0 + m + \bar{m}) \tag{25}$$

for some $A$ in $\mathbb{R}$, hence Eq. (21) is verified. Here $\hat{C}$ contains the product between $(3\sqrt{\pi}/4\rho_{gr})^{2/3}$ and $\tilde{C}$.

Verifying the initial condition is a bit more delicate. Typically in the study of dust growth, the initial condition of the size distribution is chosen to follow $n(a) \propto a^{-3.5}$ as was determined by

observations of the ISM ([Mathis et al., 1977](#) and [Kim et al., 1994](#)). Thus;

$$n(a, 0) = \frac{D}{(a_{max}^{0.5} - a_{min}^{0.5})} a^{-3.5}, \quad a \in (a_{min}, a_{max}) \tag{26}$$

with $D$ a normalising dimensionless constant derived as a function of $\rho(0)$, by plugging $n(a, 0)$ in the equation for $\rho$ (cfr. Eq. (1)):

$$\rho(0) = \frac{8}{3} \pi \rho_{gr} \frac{D}{(a_{max}^{0.5} - a_{min}^{0.5})} \left[ a^{0.5} \right]_{a_{min}}^{a_{max}}. \tag{27}$$

This then gives $D = 3\rho(0)/8\pi\rho_{gr}$. Finally, the initial dust mass density $\rho(0)$ is determined using the dust-to-gas mass ratio $R = 0.01$ ([Ormel et al., 2009](#)):

$$\rho(0) = R\mu m_H n_H \tag{28}$$

where $m_H$ is the hydrogen atom mass and $\mu$ is a dimensionless parameter, namely the atomic weight per hydrogen, set to 1.4 here. In Eq. (28) the hydrogen number density is written as $n_H$. The value of $n_H$ is a parameter often used to classify molecular clouds. Here we use $10^5$ cm$^{-3}$, a value typical for dense molecular cloud cores. The initial condition for the grain size distribution can be written as function of grain mass:

$$\hat{n}(m, 0) = \frac{D}{(a_{max}^{0.5} - a_{min}^{0.5})} \frac{a^{-5.5}}{4\pi \rho_{gr}}$$

$$= \frac{D}{(a_{max}^{0.5} - a_{min}^{0.5})} \left( \frac{1}{3} \right)^{\frac{11}{6}} (4\pi \rho_{gr})^{\frac{5}{6}} m^{-\frac{11}{6}}$$

$$= C_{in} m^{-11/6}, \quad m_{min} < m < m_{max}. \tag{29}$$

Hence, condition (22) is verified since $\hat{n}(m, t)$ is not negative and its integral with measure $(m_0 + m)dm$ is finite, being the integral of a continuous function on the limited set $(m_{min}, m_{max})$. The above reasoning could be also repeated for different assumptions on the initial power law size distribution $n(a) \propto a^{-\gamma}$. In conclusion, given the problem:

$$\frac{\partial}{\partial t} \hat{n}(m, t) = -\hat{n}(m, t) \int_0^\infty K(m, \bar{m}) \hat{n}(\bar{m}, t) \, d\bar{m}$$

$$+ \frac{1}{2} \int_0^m K(m - \bar{m}, \bar{m}) \hat{n}(\bar{m}, t) \hat{n}(m - \bar{m}, t) \, d\bar{m}, \quad (m, t) \in \mathbb{R}_+^2$$

$$\hat{n}(m, 0) = C_{in} m^{-11/6} \mathbb{1}_{(m_{min}, m_{max})}, \quad m \in \mathbb{R}_+ \tag{30}$$

a unique mass conservative solution $\bar{n}(m, t)$ exists, which satisfies Eq. (30) $\forall (m, t) \in \mathbb{R}_+^2$. In Eq. (30) $K(m, \bar{m})$ is the kernel in deterministic form computed with either the maximum or minimum relative velocity from Eqs. (15)–(16).

## 5. Conservative formulation

Following the approach of [Filbet and Laurençot (2004)](#), the Smoluchowski coagulation equation is now rewritten in its conservative hyperbolic formulation:

$$m \, \partial_t \hat{n}(m, t) = -\partial_m J(\hat{n})(m, t),$$

$$J(\hat{n})(m, t) = \int_0^m \int_{u-m}^\infty u \hat{n}(u) \hat{n}(v) K(u, v) \, dv \, du$$

$$\hat{n}(m, 0) = C_{in} m^{-11/6} \mathbb{1}_{(m_{min}, m_{max})}, \quad m \in \mathbb{R}_+ \tag{31}$$

which is suited for codes designed to solve hyperbolic equations. This conservative formulation is equivalent to the Smoluchowski set of Eq. (30) multiplied by $m$, the equivalence of which can be
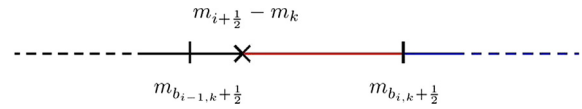


**Fig. 1.** Visual scheme to show $m_{b_{i,k}}$ subinterval. $(m_{i+1/2} - m_k, m_{b_{i,k+1/2}})$ is the integration domain of $B_{i,k}$ and $m_{b_{i,k+1/2}}$ is the beginning of the integration domain for $A_{kj}$.

shown by recursively applying the general relation

$$\partial_x \int_{h(x)}^{g(x)} f(x, y) dy = f(x, g(x)) g'(x) - f(x, h(x)) h'(x)$$

$$+ \int_{h(x)}^{g(x)} \partial_x f(x, y) dy, \tag{32}$$

to the RHS of the first equation in (31).

In [Filbet and Laurençot (2004)](#), another proposed change of function variable for a more direct observation of mass conservation is made. Since mass variable $m$ does not depend on time, it can be brought inside the partial time derivative in Eq. (31), allowing for a change in variable, from $\hat{n}(m, t)$ to $g(m, t) = m\hat{n}(m, t)$ and the problem reads:

$$\partial_t g(m, t) = -\partial_m \int_0^m \int_{m-u}^\infty K(u, v) g(u) \frac{g(v)}{v} du \, dv, \tag{33}$$

$$g(m, 0) = m C_{in} m^{-11/6} \mathbb{1}_{(m_{min}, m_{max})}, \quad m \in \mathbb{R}_+.$$

Mass is conserved if $\|g\|_{L_1}$ is constant in time.

Eq. (33) is collected in Table 3 together with the previous two formulations.

## 6. Numerical method

For the validation of the model a MATLAB code was constructed. Following [Filbet and Laurençot (2004)](#) a finite volume approach was applied, leading to the numerical problem:

$$\partial_t g_i(t) = -\frac{1}{\Delta m_i} \left[ J_{i+1/2}(t) - J_{i-1/2}(t) \right] \quad \forall i = \{1, \ldots, N\}, \, \forall t > 0 \tag{34}$$

$$g_i^0 = 6 \frac{C_{in}}{\Delta m_i} \left[ m^{1/6} \mathbb{1}_{(m_{min}, m_{max})} \right]_{m_{i-1/2}}^{m_{i+1/2}}, \quad \forall i = \{1, \ldots, N\}$$

with $\Delta m_i$ mass interval and flux at the boundary

$$J_{i+1/2}(t) = \sum_{k=1}^i \Delta m_k \, g_k(t) \left[ B_{i,k} g_{b_{i,k}}(t) + \sum_{j=b_{i,k}+1}^N A_{kj} g_j(t) \right]. \tag{35}$$

Even though in the analytical expression (33), $m \in \mathbb{R}_+$, for the code implementation an upper bound of the computational domain, $m_{top}$, has to be chosen. Given the initial distribution with support $(m_{min}, m_{max})$ (the values used in the code are $(9.5 \times 10^{-21}, 9.5 \times 10^{-12})$ g), a conservative upper value $m_{top}$ is selected such that no larger grains are formed in the time range considered (since only coagulation is considered, the grains mass will become larger and larger with time). Eventually an appropriate computational domain $(m_{min}, m_{top})$ is chosen and then divided into $N$ subintervals, indexed by $i$. The meaning of the index $b_{i,k}$ (appearing as index for some terms within the brackets of Eq. (35)) is represented in Fig. 1. The matrix $A$ and the vector $B$ (at fixed index $i$) are

$$A_{kj} = \int_{m_{j-1/2}}^{m_{j+1/2}} K(m_k, v)/v \, dv, \tag{36}$$

$$B_{i,k} = \int_{m_{i+1/2} - m_k}^{m_{b_{i,k+1/2}}} K(m_k, v)/v \, dv. \tag{37}$$

For the time derivative, an explicit Euler scheme is chosen, with a time step stability constraint relaxed with respect to the one proposed in Filbet and Laurençot (2004), to the expression

$$\Delta t \left[ \sup_{i,n} g_1^n \int_{m_1}^{m_{1+1/2}} \frac{K(m_i, m)}{m} \, dm \right.$$
$$\left. + \sum_{k=2}^{N} g_k^n \int_{m_{k-1/2}}^{m_{k+1/2}} \frac{K(m_i, m)}{m} \, dm \right] < 1. \quad (38)$$

In the Appendix the analytical proof of this relaxation is shown in detail. The practical effect is that the upper limit for the time step goes from 12 h to $10^5$ years, on a simulation of the order of $10^6$ years, which means going from $10^8$ to just 10–20 time iterations. One can also verify the stability of the method with numerical experiments using different timesteps, and all our numerical results adopted this constraint.

Finally, for the boundary conditions, the underlying assumption is that $g$ is zero for $m < m_{min}$, since through coagulation the grains can only grow bigger, moreover no grains bigger than $m_{top}$ are created and therefore $g$ is again zero for $m > m_{top}$. The latter can be verified by numerically computing the outflow flux $J_{N+1/2}$.

Eq. (35) is the last reformulation for the coagulation model to appear in Table 3.

## 7. Numerical results

The coagulation model by Hirashita has been presented, its continuous formulation has been derived and analysed from a mathematical point of view and ultimately rewritten in a conservative form, following the work of Filbet and Laurençot (2004). The core of all models is the Smoluchowski coagulation equation with a particular kernel to describe the specific physics of the phenomenon. Two possible numerical implementations were also presented, one is the initial discrete model itself, the other has been derived from the conservative formulation in the previous section. Hereafter the two methods implemented in MATLAB are tested and compared. They will be referred to as the *discrete* model:

$$\begin{cases} \dfrac{\rho_i^{n+1} - \rho_i^n}{\Delta t} = m_i \rho_i \sum_{l=1}^{N} \alpha_{li} \rho_l + \sum_{j=1}^{N} \sum_{l=1}^{N} \alpha_{lj} \rho_l \rho_j m_{coag}^{lj}(i), \\ \rho_i^0 = C_{in} m_i^{-5/6} \Delta m_i, \end{cases} \quad (39)$$

and the *conservative* model:

$$\begin{cases} g_i^{n+1} = g_i^n - \dfrac{\Delta t}{\Delta m_i} \left[ J_{i+1/2}^n - J_{i-1/2}^n \right], \\ g_i^0 = 6 \dfrac{C_{in}}{\Delta m_i} \left[ m^{1/6} \mathbb{1}_{(m_{min}, m_{max})} \right]_{m_{i-1/2}}^{m_{i+1/2}}. \end{cases} \quad (40)$$

Both have cell (grain size bin) index $i = \{1, \ldots, N\}$ and time levels indicated by $n = \{0, \ldots, M - 1\}$. The two models differ in their unknowns, since the *discrete* one controls the evolution of the total dust mass density contained in each bin ($\rho_i$), whereas the other looks at the average dust mass density $g_i$ of the $i$th bin:

$$\rho_i^n = \hat{n}(m_i, t_n) m_i \Delta m_i, \qquad g_i^n = \frac{1}{\Delta m_i} \int_{m_{i-1/2}}^{m_{i+1/2}} \hat{n}(m_i, 0) m_i \, dm. \quad (41)$$

Therefore, a quantity that allows to compare the codes directly is the total volume/mass occupied by the bins,

$$f_i^n = a_i^4 \frac{n(a_i, t_n)}{n_H} = \frac{9 m_i^2}{4 \pi \rho_{gr}} \frac{\hat{n}(m_i, t_n)}{n_H}. \quad (42)$$
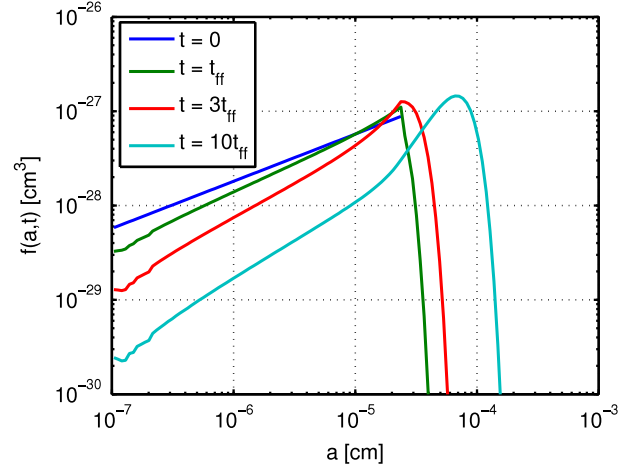


**Fig. 2.** Simulation with stochastic kernel, obtained using $N = 128$ and $dt = 10$ yr, showing the time evolution of $f(a, t)$.

The parameters used to match values typical for molecular clouds are listed in Table 1. The size of the grains is discretised with an exponential grid:

$$a_{i+1/2} = a_{i-1/2} \delta, \qquad a_i = \frac{a_{i+1/2} - a_{i-1/2}}{2}, \quad i \in \{1, \ldots, N\}. \quad (43)$$

Where $a_{1/2} = a_{min}$ in order to treat the initial left boundary layer, $\delta = (a_{top}/a_{min})^{1/N}$ and, as a result, $a_{N+1/2} = a_{top}$. The respective quantities for the mass are obtained with the relation $m = (4/3)\pi \rho_{gr} a^3$. $N$ can be chosen arbitrarily, and here it will take one of the values $\{8, 16, 32, 64, 128\}$, while the results in Hirashita and Li (2013) use $N = 128$.

For what concerns the time, the typical scale is the free-fall time $t_{ff}$ which is the time within which the molecular cloud collapses under its own gravitational attraction if no other forces exist to oppose the collapse,

$$t_{ff} = \sqrt{\frac{3\pi}{32 \, G \, \mu \, m_H \, n_H}} = 1.38 \times 10^5 \text{ yr}, \quad (44)$$

with $G$ the gravitational constant. The typical setup is run up to $10 t_{ff}$, with a time step that ranges from 10 to 100 years.

### 7.1. Validation of the code

Validation of the code is not straightforward. The matching with Hirashita's results should be the starting point, but with the continuous formalism the stochastic process was substituted with the maximum or minimum relative velocity, and therefore the results are not directly comparable. To solve this issue, the *discrete* code is initially run with the stochastic kernel and this is shown in Fig. 2. This matches Hirashita's results in a recent erratum (Hirashita and Li, 2014), which reports the corrected simulations of Hirashita and Li (2013). In the remainder of this paper, the deterministic maximum and minimum kernel will always be used in the *discrete* model, and will be referred to as $H_{max,min}$.

### 7.2. Comparing the discrete and conservative cases

At this point the *discrete* code is run with the maximum and minimum kernel, to be compared with the results obtained with the *conservative* code. When the resolution is high, i.e. the size refinement goes up to $N = 128$ and the time step is small (100 years or less), the output of the two codes overlap both
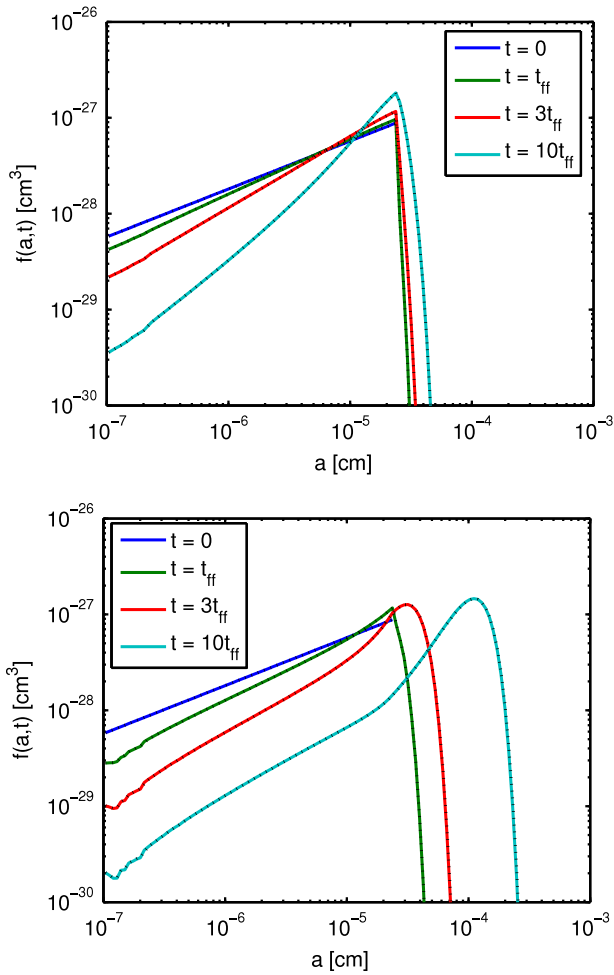
**Fig. 3.** Overlap in the results from discrete (in colour with solid line) and *conservative* (black dotted line) codes at four different times in the evolution. The outputs are for minimum (top) and maximum (bottom) kernels. $N = 128$, $dt = 100$ yr. (For interpretation of the references to colour in this figure legend, the reader is referred to the web version of this article.)

**Fig. 4.** First order time convergence. The relative errors of Table 2 for maximum kernels are plotted in a logarithmic graph, the linear behaviour confirms the explicit Euler scheme accuracy.

for the minimum and the maximum kernel (see Fig. 3). It is interesting to notice from an astrophysical point of view that with the maximum kernel above $10t_{\text{ff}}$ the peak of the mass distribution is at 1 μm, which means that 1 μm grains constitute the majority of the mass. A similar distribution would be consistent with the coreshine phenomenon observed in molecular clouds, where stars are formed.
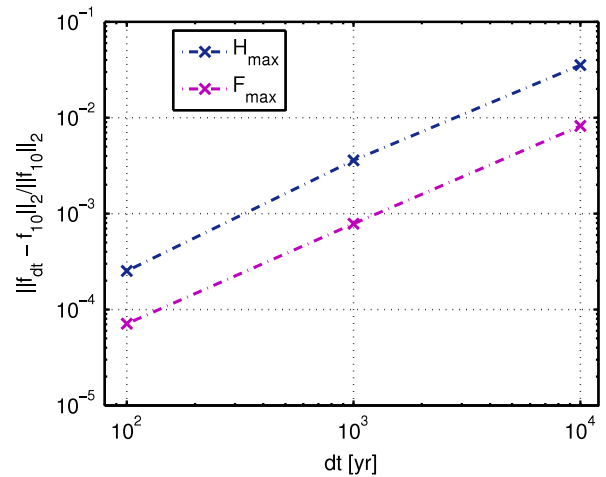
To gain confidence in the models and understand better how the time step and the number of bins influence the results, the numerical convergence is studied by testing various settings.

### 7.3. Time convergence

An estimate of the relative error is done to compare the time convergence performances. The exact solution is approximated with the most refined result computed ($dt = 10$ yr, $N = 128$), namely

$$\text{err}_{dt} = \frac{\|f_{dt} - f_{10}\|_2}{\|f_{10}\|_2} = \frac{\left(\sum_{i=1}^{N}(f_i^{dt} - f_i^{10})^2 da_i\right)^{1/2}}{\left(\sum_{i=1}^{N}(f_i^{10})^2 da_i\right)^{1/2}}, \qquad (45)$$

where the suffix 2 indicates the $\mathbb{L}_2$ norm. In Table 2, the errors at $t = 10t_{\text{ff}}$ are reported for the two codes and both kernels, high-lighting that the code is very stable in time and the performance

of the *conservative* code for the maximal velocity is almost one order of magnitude better than the *discrete* one. By representing the values with a logarithmic plot (Fig. 4 for maximal kernel), the first order convergence given by the explicit Euler method is recovered for both models. Obviously, one may now extend the temporal accuracy in standard ways (using multistep approaches), but this is left for future work. Second order accuracy has e.g. been shown for the conservative method in Filbet and Laurençot (2004).

### 7.4. Changing number of bins

With the aim of expanding these equations to the scenario where space dependence is also taken into account (for example as part of a full fluid simulation), avoiding excessive computational cost is important, and testing the code for coarser grids is essential. A high number of bins does not only bring additional cost to solve the coagulation process, but has a great impact on the dust to gas coupling as well as when the resulting aim is to add dust growth to the dynamical simulations. It is therefore important to have good numerical behaviour even when the grid is coarse.

As can be seen in Fig. 5, the *conservative* model is quite robust for low number of bins, while the output of the *discrete* one for $N = 8$ and $N = 16$, does not resemble the desired profile. More quantitatively, along the lines of what was done for the time convergence, it is possible to estimate the error in the $\mathbb{L}_2$ norm. The numerical computation is complicated by the fact that the grid discretisation changes and there is no unique $N$ in Eq. (45). To overcome this problem, the final distributions are projected on a finer grid ($N = 1000$) and Eq. (45) is used with $N = 1000$, the exact solution is now approximated with the final distribution for $N = 128$ and $dt = 100$ yr.

In Fig. 6 the relative errors,

$$\text{err}_N = \frac{\|f_N - f_{128}\|_2}{\|f_{128}\|_2} \qquad (46)$$

are shown for simulations with 8 to 80 bins. Unlike the time convergence, the errors are not aligned but they do follow a linearly decreasing pattern. A regression line is plotted to highlight this behaviour, with slopes of 1.07 for the *discrete* and 0.88 for the *conservative* cases, leading to a slightly lower magnitude of error. By looking at the vertical axis, the relative errors range from 0.1 to 0.9. Considering that the errors for $dt = 10^4$ yr were of the order $10^{-3}$–$10^{-2}$ (Table 2), it can be stated that both methods behave considerably better in time than in space.

**Table 2**
This table gathers estimated relative errors in $L_2$ norm for the final distributions ($N = 128$). The values for *discrete* $H_{max,min}$ and *conservative* $F_{max,min}$ computations are reported, where maximal or minimal kernels are adopted, for different time step choices.

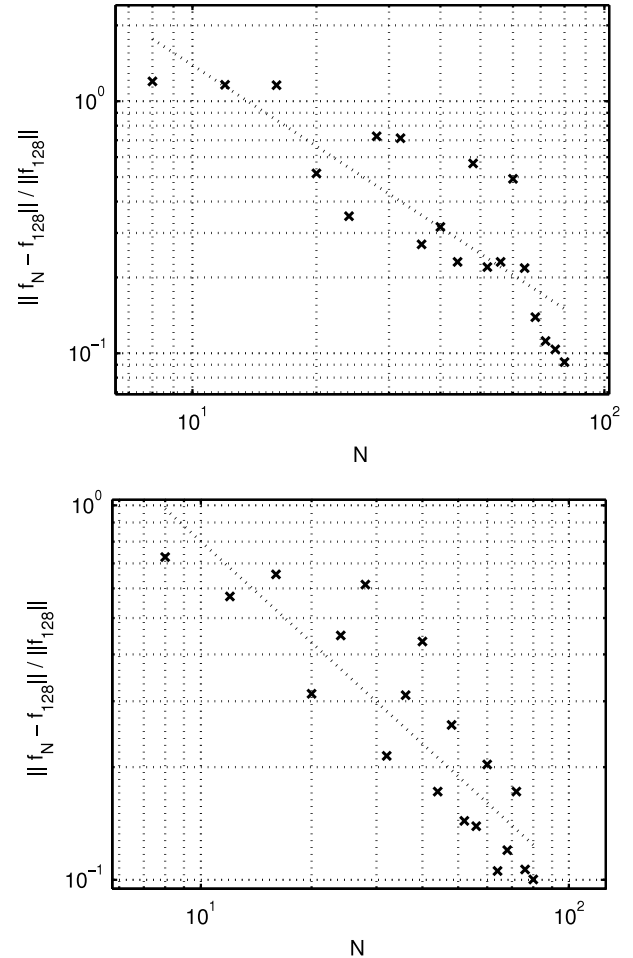| | $F_{max}$ | $H_{max}$ | $F_{min}$ | $H_{min}$ |
|---|---|---|---|---|
| $dt = 10^2$ [yr] | $7.11 \times 10^{-5}$ | $2.53 \times 10^{-4}$ | $2.99 \times 10^{-5}$ | $2.87 \times 10^{-5}$ |
| $dt = 10^3$ [yr] | $7.85 \times 10^{-4}$ | $3.60 \times 10^{-3}$ | $3.29 \times 10^{-4}$ | $5.89 \times 10^{-4}$ |
| $dt = 10^4$ [yr] | $8.21 \times 10^{-3}$ | $3.54 \times 10^{-2}$ | $3.32 \times 10^{-3}$ | $5.32 \times 10^{-3}$ |
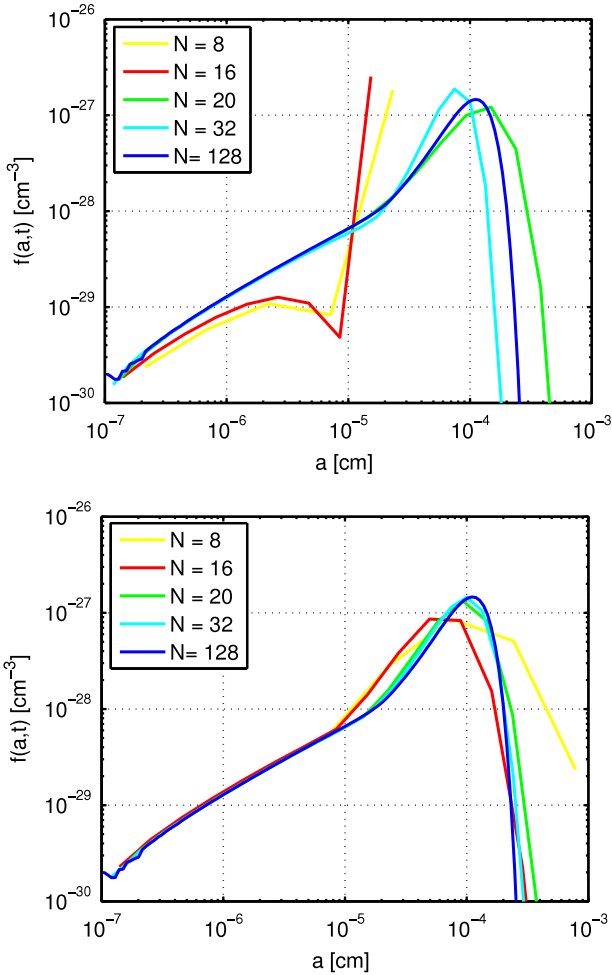


**Fig. 5.** Behaviour for low number of bins for *discrete* (top) and *conservative* (bottom) codes for maximum final distribution ($dt = 100$ yr). The continuous code performs better with coarser grids.



**Fig. 6.** *Discrete* (top) and *conservative* (bottom) logarithmic error plot ($dt = 100$ yr). $X$ indicates the actual error values, while the dotted line is obtained through linear regression.

### 7.5. Mass conservation

While discussing the property of the Smoluchowski coagulation equation with Hirashita's kernel (Section 4), it was proven that the initial condition and the maximum and minimum kernels were such that the mass was (analytically) conserved. Here mass conservation is tested numerically. Fig. 7 shows that both kernels conserve mass, but the *conservative* scheme has a performance which is three orders of magnitude better. The values plotted are the relative difference in mass between time 0 and time $10t_{ff}$, showing no specific pattern when $N$ changes.

## 8. Conclusions

The equivalence between the *discrete* coagulation model and the Smoluchowski continuous formulation has been proved and the kernel identified. With the specific kernel and initial condition

it was possible to analytically infer existence of a unique, mass conserving solution. The continuous model, rewritten in the conservative form, allowed the use of a finite-volume discretisation, and both numerical approaches were demonstrated to produce mass conserving evolutions. Numerical properties such as convergence in the temporal as well as in the grain size bin discretisation were analysed. For the latter, it was shown that even a fairly coarse bin size distribution can yield satisfactory results of coagulation processes when the *conservative* formulation is used. This is of interest for future work, where we target spatio-temporally evolving gas–dust mixtures in molecular cloud contexts. All the different reformulations for the coagulation model are gathered in Table 3. Besides dynamic coupling through drag-forces as was done to date, the present work paves the way to create a method that also accounts for coagulation processes in the dust distribution, thereby extending work like Birnstiel et al. (2010) to full 3D dynamical computations.

When one wants to enrich a 3D fluid code with dust evolution and coagulation, the additional computational cost will come
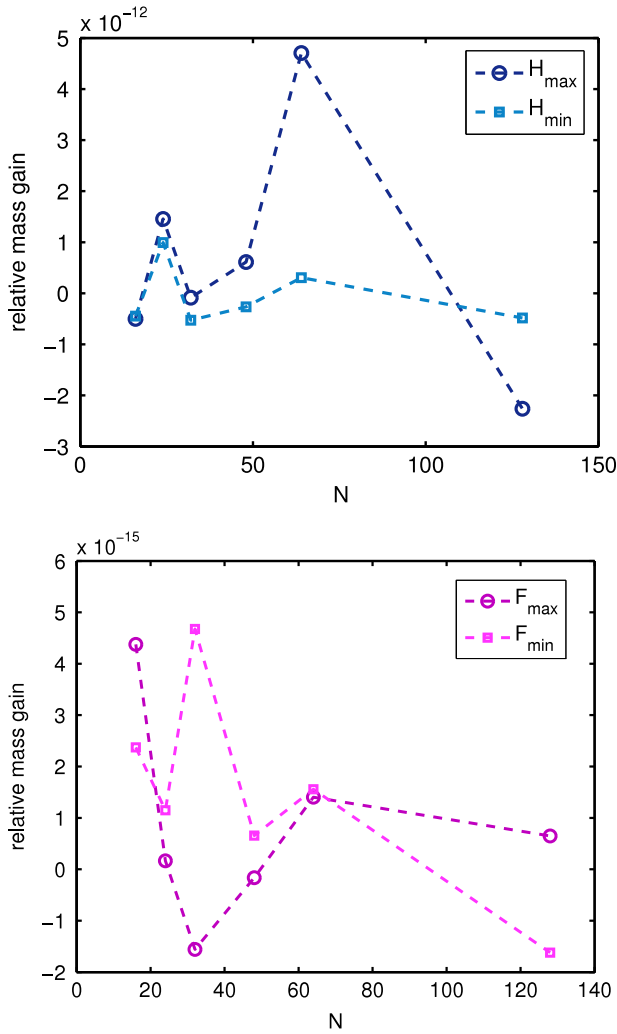
**Fig. 7.** Relative mass gain for the *discrete* (top) and the *conservative* (bottom) codes for maximum and minimum kernels ($dt = 100$ yr). Both methods show conservation of mass (note the scale factor, going to near machine precision) independent of the number of bins, but the first has an accuracy of $10^{-12}$, while the second has $10^{-15}$.

**Table 3**

A collection of all the possible formulations of the same dust coagulation model presented within this paper. From top to bottom: the discrete form from Hirashita, the continuous Smoluchowski equation, the conservative continuous and also the conservative discrete form. Each equation and notation is explained in the corresponding sections from top to bottom: 2, 3, 5 and 6.

| Coagulation models |
|---|
| $\frac{\rho_i^{n+1}-\rho_i^n}{\Delta t} = -m_i \rho_i \sum_{l=1}^{N} \alpha_{li}\rho_l - \sum_{j=1}^{N}\sum_{l=1}^{N} \alpha_{lj}\rho_l\rho_j m_{coag}^{lj}(i)$ |
| $\frac{\partial}{\partial t}\hat{n}(m,t) = -\hat{n}(m,t)\int_0^{\infty} K(m,\bar{m})\hat{n}(\bar{m},t)\,d\bar{m}$ $\qquad + \frac{1}{2}\int_0^m K(m-\bar{m},\bar{m})\hat{n}(\bar{m},t)\hat{n}(m-\bar{m},t)\,d\bar{m}$ |
| $\partial_t g(m,t) = -\partial_m \int_0^m \int_{m-u}^{\infty} K(u,v)g(u)\frac{g(v)}{v}\,du\,dv$ |
| $g_i^{n+1} = g_i^n - \frac{\Delta t}{\Delta m_i}\left[J_{i+1/2}^n - J_{i-1/2}^n\right]$ |
| $J_{i+1/2}(t) = \sum_{k=1}^{i} \Delta m_k g_k(t)\left[B_{i,k}g_{b_{i,k}}(t) + \sum_{j=b_{i,k}+1}^{N} A_{kj}g_j(t)\right]$ |

mainly from resolving the spatial dynamics of dust rather than its coagulation. The coagulation process has a characteristic time scale much longer than the one required to resolve the gas–dust turbulent dynamics, and the rebinning can be performed locally on every single spatial cell. By suitably exploiting these

two aspects (for example by highly parallelising the code), the computational cost for the coagulation can be greatly reduced and made comparable to the one of the simulations reported in this paper, which are all feasible on laptops or desktops within minutes. Their cost is set by (a power of) the number of mass intervals adopted, along with the time step criterion as expressed by our Eq. (38). This cost is marginal compared to the cost needed for full 3D dynamical gas plus dust evolutions, where we are restricted by the usual CFL condition on the time step in explicit schemes, and by a desire to spatially resolve a significant fraction of the inertial range when turbulent conditions prevail (requiring massively parallel computations, also for gas–dust coupled settings, as reported in Porth et al. (2014)). A simulation of 3D coupled gas–dust evolutions without accounting for coagulation processes, such as that by Hendrix et al. (2015) for the Kelvin–Helmholtz ripples seen in infrared images of the Orion nebula, using block-adaptive meshes to achieve effective resolutions of $448 \times 1792 \times 448$ grid cells (in a $0.33\,\mathrm{pc}^3$ volume) and followed for order $10^5$ years, requires heavy supercomputer resources (hours to days on hundreds of processors). In such scenarios the number of bins used is of crucial importance for determining the cost. These considerations will become clearer only when an actual investigation is carried out on coupled gas–dust with evolving dust size distributions.

Finally, although we purposely discussed the specific coagulation model as used in discrete form by Hirashita (2012), and adopted parameters typical for molecular cloud cores, we gave all details needed for adapting the same approach to more advanced coagulations models. These have typically been pioneered in protoplanetary disk context, where ultimately centimetre-sized aggregates are desired, that may settle towards the disk mid-plane and form the seeds for planetesimal formation through further gravitational instability (e.g., Ormel and Cuzzi, 2007; Nomura and Nakagawa, 2006). Further realism can be expected when studying truly coupled gas–dust or plasma–dust mixtures (involving magnetohydrodynamics turbulence and the complexity of charging dust particles), an aspect that has been studied e.g. by Yan et al. (2004). Note that we have, following closely Hirashita (2012), also made very simple assumptions on the prevailing particle velocity behaviour with size, our Eq. (7). More recent insights have been acquired for collisional growth in protoplanetary disks, where Windmark et al. (2012) and Garaud et al. (2013) have pioneered the use of probability distribution functions that include both deterministic motions (settling, drifts) and stochastic motions (due to turbulence and Brownian motion). This has alleviated the barrier problem and allowed even emergence of metre to decametre sized objects, while maintaining a considerable long-term micrometre sized grain population.

### Acknowledgements

### Appendix

*Time discretisation and stability condition*

The explicit Euler scheme can be unstable if the chosen time step $\Delta t$ is not small enough. Filbet and Laurençot (2004) proposes

the following stability condition:

$$\Delta t \sup_{i,n} \left( \int_{m_{min}+\delta m}^{m_{top}} \frac{K(m_i, m)}{m} g(m, t_n)\, dm \right) < 1. \tag{47}$$

Where $\delta m = \min_i \Delta m_i / 2$, which for the kind of exponential bin discretisation used for this work coincides with $\Delta m_1/2$.

In fact, within this context, this stability constraint can be relaxed to

$$\Delta t \sup_{i,n} \left( \int_{m_{i+1/2}-m_i}^{m_{top}} \frac{K(m_i, m)}{m} g(m, t_n)\, dm \right) < 1. \tag{48}$$

In essence, Filbet takes the maximum integration interval $(m_{min} + \delta m, m_{top})$ and then finds the supremum of the function on that fixed interval, whereas, to carry out the proof, it is not necessary to decouple the domain length from the function. This difference becomes considerable when using Hirashita's kernel, as the relaxation permits the time step constraint to change from a day to a million years.

The new estimate can therefore be proven by following the same proof found in Filbet, presented below with a slight difference in notation, to be consistent with the work done so far. The proof is split into two propositions.

**Proposition 1.** *Given the continuous problem*

$$\partial_t g(m, t) = -\partial_m J(g)(m, t), \quad (t, m) \in (\mathbb{R}^+ \times (m_{min}, m_{top}))$$

$$J(g)(m, t) = \int_{m_{min}}^{m} \int_{m-u}^{m_{top}} \frac{K(u, v)}{v} g(v)g(u)\,dv\,du,$$

$$g(m, 0) = mC_{in}m^{-11/6}\chi_{(m_{min},m_{max})}, \quad m \in (m_{min}, m_{top})$$

$$J(g)(m_{min}, t) = 0, \quad t \in \mathbb{R}^+ \tag{49}$$

*and given its numerical approximation:*

$$g_i^{n+1} = g_i^n - \frac{\Delta t}{\Delta m_i}\left[ J_{i+1/2}^n - J_{i-1/2}^n \right]$$

$$\forall i = \{1, \ldots, N\}, \ \forall n = \{0, \ldots, M\text{-}1\}$$

$$J_{i+1/2}^n = \sum_{k=1}^{i} \Delta m_k\, g_k^n \left[ B_{i,k}g_{b_{i,k}}^n + \sum_{j=b_{i,k}+1}^{N} A_{kj}g_j(t) \right]$$

$$g_i^0 = 6C_{in}\left[ m^{1/6}\chi_{(m_{min},m_{max})} \right]_{m_i^{(l)}}^{m_i^{(r)}} \quad \forall i = \{1, \ldots, N\}$$

$$J_{1/2}^n = 0 \quad 0 q d \forall i = \{1, \ldots, N\}, \tag{50}$$

*then the following relation for the fluxes holds:*

$$J_{i+1/2}^n - J_{i-1/2}^n \le \Delta m_i g_i^n \left[ B_{i,i}g_{b_{i,i}}^n + \sum_{j=b_{i,i}+1}^{N} A_{ij}g_j^n \right]. \tag{51}$$

*where $K(u, v)$ is a symmetric positive kernel in both $(u, v)$ and the discrete expressions for A and B are:*

$$A_{kj} = \int_{m_{j-1/2}}^{m_{j+1/2}} K(m_k, v)/v\, dv \tag{52}$$

$$B_{i,k} = \int_{m_{i+1/2}-m_k}^{m_{b_{i,k}+1/2}} K(m_k, v)/v\, dv, \tag{53}$$

*with $b_{i,k}$ index chosen such that $m_{i+1/2} - m_k$ belongs to its interval (as showed in Fig. 1).*

**Proof.** Throughout the computation the assumption $g^n$ non-negative ($g_0 \ge 0$) is used. Starting from the equation for $J_{i+1/2}$

in (50)

$$J_{i+1/2}^n = \sum_{k=1}^{i} \Delta m_k g_k^n \left[ \sum_{j=b_{i,k}+1}^{N} A_{kj}g_j^n + B_{i,k}g_{b_{i,k}}^n \right]$$

$$= \Delta m_i g_i^n \left[ \sum_{j=b_{i,i}+1}^{N} A_{ij}g_j^n + B_{i,i}g_{b_{i,i}}^n \right]$$

$$+ \sum_{k=1}^{i-1} \Delta m_k g_k^n \left[ \sum_{j=b_{i,k}+1}^{N} A_{kj}g_j^n + B_{i,k}g_{b_{i,k}}^n \right], \tag{54}$$

where in the second passage the sum from 1 to $i$ has been split in the sum till $i-1$ plus the terms in $i$. Now the aim is to recover from the first sum the left flux at $i-1/2$. In the case that $b_{i-1,k} = b_{i,k}$, Eq. (54) results in:

$$J_{i+1/2}^n = \Delta m_i g_i^n \left[ \sum_{j=b_{i,i}+1}^{N} A_{ij}g_j^n + B_{i,i}g_{b_{i,i}}^n \right]$$

$$+ \sum_{k=1}^{i-1} \Delta m_k g_k^n \left[ \sum_{j=b_{i-1,k}+1}^{N} A_{kj}g_j^n + B_{i,k}g_{b_{i-1,k}}^n \right]. \tag{55}$$

As Filbet points out, if $b_{i-1,k} = b_{i,k}$ then $B_{i,k} \le B_{i-1,k}$, because in fact $B_{i,k}$ is an integral on the domain $(m_{i+1/2} - m_k, m_{b_{i,k}-1/2})$, while $B_{i-1,k}$ operates on the wider interval $(m_{i-1/2} - m_k, m_{b_{i,k}-1/2})$. The second term at the right hand side is therefore less than $J_{i-1/2}^n$, leading to the desired inequality (51).

Whereas if $b_{i-1,k} < b_{i,k}$, (note that the inverse inequality can never be verified), the internal sum of the last term in Eq. (54) is rewritten

$$\sum_{j=b_{i,k}+1}^{N} A_{kj}g_j^n = \sum_{j=b_{i-1,k}+1}^{N} A_{kj}g_j^n - \sum_{j=b_{i-1,k}+1}^{b_{i,k}} A_{kj}g_j^n, \tag{56}$$

$$J_{i+1/2}^n \le \Delta m_i g_i^n \left[ \sum_{j=b_{i,i}+1}^{N} A_{ij}g_j^n + B_{i,i}g_{b_{i,i}}^n \right]$$

$$+ \sum_{k=1}^{i-1} \Delta m_k g_k^n \left[ \sum_{j=b_{i-1,k}+1}^{N} A_{kj}g_j^n + B_{i-1,k}g_{b_{i-1,k}}^n \right]$$

$$+ \sum_{k=1}^{i-1} \Delta m_k g_k^n \left[ \sum_{j=b_{i-1,k}+1}^{b_{i,k}} -A_{kj}g_j^n + B_{i,k}g_{b_{i,k}}^n \right]. \tag{57}$$

$B_{i-1,k}g_{b_{i-1,k}}^n$ was added, being a non-negative term, in order to recover $J_{i-1/2}$ in the second line. The only thing left to prove to obtain Eq. (51), is that the third term at the right hand side is negative.

$$\sum_{j=b_{i-1,k}+1}^{b_{i,k}} A_{kj}g_j^n = \int_{m_{b_{i-1,k}+1/2}}^{m_{b_{i,k}+1/2}} \frac{K(m_k, v)}{v} g(v)\, dv$$

$$\ge \int_{m_{i+1/2}-m_k}^{m_{b_{i,k}+1/2}} \frac{K(m_k, v)}{v} g(v)\, dv = B_{i,k}g_{b_{i,k}}^n. \tag{58}$$

**Proposition 2.** *Given the validity of Proposition 1, then for any time step $\Delta t$ that satisfies the stability condition (48) it can be proven that:*

- $g_i^n$ *is non-negative for all i,*
- $\sum_{i=1}^{N} g_i^{n+1} \le \sum_{i=1}^{N} g_i^n,$

*for all* $n \in (1..M)$. *The physical meaning of these results is that the number density solution is non-negative and that the total mass is non-increasing in time. The latter coincides with the stability condition in norm* $L_1$: $\|g^{n+1}\|_{L^1} \leq \|g^n\|_{L^1}$.

**Proof.** The stability condition (48) for $\Delta t$ can be rewritten using $A$ and $B$

$$\Delta t \sup_{i,n} \left[ B_{i,i} g_{b_{i,i}}^n + \sum_{j=b_{i,i}+1}^{N} A_{ij} g_j^n \right] < 1. \tag{59}$$

Then Eq. (51) becomes:

$$J_{i+1/2}^n - J_{i-1/2}^n \leq \frac{\Delta m_i}{\Delta t} g_i^n, \quad \forall i, n. \tag{60}$$

Hence $g_i^{n+1}$ is non-negative, since

$$g_{i+1}^n = g_i^n - \frac{\Delta t}{\Delta m_i} \left( J_{i+1/2}^n - J_{i-1/2}^n \right). \tag{61}$$

Finally, to recover the time monotonicity of the total mass, Filbet claims that (on an infinitive domain) it comes directly from the non-negativity of $g^n$ and from summing the above equation over $i$. Using the boundary conditions:

$$\sum_{i=1}^{N} \Delta m_i g_i^{n+1} = \sum_{i=1}^{N} \Delta m_i g_i^n - (J_{N+1/2}^n - J_{1/2}^n). \tag{62}$$

$J_{N+1/2}^n - J_{1/2}^n$ has to be $\geq 0$ for all $n$, which is guaranteed by the non-negativity of the flux and the boundary condition $J_{1/2}^n = 0$.

## References

Birnstiel, T., Dullemond, C.P., Brauer, F., 2010. Gas- and dust evolution in protoplanetary disks. A&A 513, A79. doi:10.1051/0004-6361/200913731, arXiv:1002.0335.

Dubovskiĭ, P.B., 1994. Mathematical Theory of Coagulation. National Univ.

Filbet, F., Laurençot, P., 2004a. Mass-conserving solutions and non-conservative approximation to the Smoluchowski coagulation equation. Arch. Math 83, 558–567.

Filbet, F., Laurençot, P., 2004. Numerical simulation of the Smoluchowski coagulation equation. SIAM J. Sci. Comput. 25, 2004b–2028.

Garaud, P., Meru, F., Galvagni, M., Olczak, C., 2013. From dust to planetesimals: An improved model for collisional growth in protoplanetary disks. Astrophys. J. 764, 146. doi:10.1088/0004-637X/764/2/146, arXiv:1209.0013.

Hendrix, T., Keppens, R., 2014. Effect of dust on Kelvin-Helmholtz instabilities. A&A 562, A114. doi:10.1051/0004-6361/201322322.

Hendrix, T., Keppens, R., 2015. Modelling colliding wind binaries in 2D. In: W.-R. Hamann, A. Sander, H. Todt, (Eds.) Wolf-Rayet Stars: Proceedings of an International Workshop held in Potsdam, Germany, 1–5 June 2015. Edited by Wolf-Rainer Hamann, Andreas Sander, Helge Todt. Universitätsverlag Potsdam, 2015., 2015, pp. 279–282.

Hendrix, T., Keppens, R., Camps, P., 2015. Modelling ripples in orion with coupled dust dynamics and radiative transfer. A&A 575, A110. doi:10.1051/0004-6361/201425498, arXiv:1502.04011.

Hirashita, H., 2012. Dust growth in the interstellar medium: how do accretion and coagulation interplay? Mon. Not. R. Astron. Soc. 422, 1263–1271.

Hirashita, H., Li, Z.-Y., 2013. Condition for the formation of micron-sized dust grains in dense molecular cloud cores. Monthly Notices of the Royal Astronomical Society 434, L70–L74.

Hirashita, H., Li, Z.-Y., 2014. Condition for the formation of micron-sized dust grains in dense molecular cloud cores. Monthly Notices of the Royal Astronomical Society 442 (2), 1661–1662 (erratum).

Hirashita, H., Yan, H., 2009. Shattering and coagulation of dust grains in interstellar turbulence. Monthly Notices of the Royal Astronomical Society 394, 1061–1074.

Kim, S.-H., Martin, P., Hendry, P.D., 1994. The size distribution of interstellar dust particles as determined from extinction. Astrophys. J. 422, 164–175.

Laibe, G., Price, D.J., 2012. Dusty gas with smoothed particle hydrodynamics— I. Algorithm and test suite. Mon. Not. R. Astron. Soc. 420, 2345–2364. doi:10.1111/j.1365-2966.2011.20202.x, arXiv:1111.3090.

Mathis, J.S., Rumpl, W., Nordsieck, K.H., 1977. The size distribution of interstellar grains. Astrophys. J. 217, 425–433.

Miniati, F., 2010. A hybrid scheme for gas-dust systems stiffly coupled via viscous drag. J. Comput. Phys. 229, 3916–3937. doi:10.1016/j.jcp.2010.01.034, arXiv:1001.4794.

Nomura, H., Nakagawa, Y., 2006. Dust size growth and settling in a protoplanetary disk. ApJ 640, 1099–1109. doi:10.1086/500251, arXiv:astro-ph/0601013.

Okuzumi, S., Tanaka, H., Sakagami, M.-A., 2009. Numerical modeling of the coagulation and porosity evolution of dust aggregates. ApJ 707, 1247–1263. doi:10.1088/0004-637X/707/2/1247, arXiv:0911.0239.

Ormel, C.W., Cuzzi, J.N., 2007. Closed-form expressions for particle relative velocities induced by turbulence. Astron. Astrophys. 466, 413–420.

Ormel, C.W., Paszun, D., Dominik, C., Tielens, A.G.G.M., 2009. Dust coagulation and fragmentation in molecular clouds. I. How collisions between dust aggregates alter the dust size distribution. Astron. Astrophys. 502, 845–869.

Ormel, C.W., Spaans, M., Tielens, A.G.G.M., 2007. Dust coagulation in protoplanetary disks: porosity matters. A&A 461, 215–232. doi:10.1051/0004-6361:20065949, arXiv:astro-ph/0610030.

Paardekooper, S.-J., Mellema, G., 2006. Dust flow in gas disks in the presence of embedded planets. A&A 453, 1129–1140. doi:10.1051/0004-6361:20054449, arXiv:astro-ph/0603132.

Pagani, L., Steinacker, J., Bacmann, A., Stutz, A., Henning, T., 2010. The ubiquity of micrometer-sized dust grains in the dense interstellar medium. Science 329, 1622. doi:10.1126/science.1193211.

Porth, O., Xia, C., Hendrix, T., Moschou, S.P., Keppens, R., 2014. MPI-AMRVAC for solar and astrophysics. Astrophys. J. Suppl. 214, 4. doi:10.1088/0067-0049/214/1/4, arXiv:1407.2052.

Saito, T., 2002. Numerical analysis of dusty-gas flows. J. Comput. Phys. 176, 129–144. doi:10.1006/jcph.2001.6971.

Smoluchowski, M.V., 1916. Drei vortrage uber diffusion, brownsche bewegung und koagulation von kolloidteilchen. Z. Phys. 17, 557–585.

Spitzer Jr., L., 1954. Behavior of matter in space. ApJ 120, 1. doi:10.1086/145876.

Steinacker, J., Pagani, L., Bacmann, A., Guieu, S., 2010. Direct evidence of dust growth in L183 from mid-infrared light scattering. A&A 511, A9. doi:10.1051/0004-6361/200912835.

Suttner, G., Yorke, H.W., 2001. Early dust evolution in protostellar accretion disks. ApJ 551, 461–477. doi:10.1086/320061, arXiv:astro-ph/0012450.

Testi, L., Birnstiel, T., Ricci, L., Andrews, S., Blum, J., Carpenter, J., Dominik, C., Isella, A., Natta, A., Williams, J.P., Wilner, D.J., 2014. Dust evolution in protoplanetary disks. Protostars Planets VI, 339–361. doi:10.2458/azu_uapress_9780816531240-ch015, arXiv:1402.1354.

Windmark, F., Birnstiel, T., Ormel, C.W., Dullemond, C.P., 2012. Breaking through: The effects of a velocity distribution on barriers to dust growth. A&A 544, L16. doi:10.1051/0004-6361/201220004, arXiv:1208.0304.

Yan, H., Lazarian, A., Draine, B.T., 2004. Dust dynamics in compressible magnetohydrodynamic turbulence. Astrophys. J. 616, 895–911.